Journal of Energy Storage 74 (2023) 109359

Contents lists available at ScienceDirect

Journal of Energy Storage

journal homepage: www.elsevier.com/locate/est

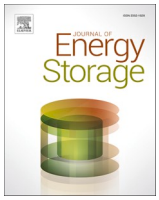

Research papers

Experimental evaluation of different macro-encapsulation designs for PCM storages for cooling applications

Omais Abdur Rehman [a,b], Valeria Palomba [a], David Verez [b,c], Emiliano Borri [b], Andrea Frazzica [a], Vincenza Brancato [a], Teresa Botargues [d], Zafer Ure [e], Luisa F. Cabeza [b,*]

[a] National Research Council of Italy – Institute for Advanced Energy Technologies (CNR-ITAE), Salita S.Lucia sopra Contesse 5, 98126 Messina, Italy
[b] GREiA Research Group, Universitat de Lleida, Pere de Cabrera s/n, 25001 Lleida, Spain
[c] ARCbcn enginyers consultors, Pau Claris 97, 1-2, 08009 Barcelona, Spain
[d] USER FEEDBACK PROGRAM SL, Sant Jaume Apòstol 8, 25126 Almenar, Spain
[e] Phase Change Material Products Limited, Yaxley, Cambridgeshire, United Kingdom

ARTICLE INFO

Keywords:
Thermal energy storage
Macro-encapsulation designs
Phase change material (PCM)
Experimental study
Cooling applications

ABSTRACT

Extensive research has been conducted on utilizing phase change materials for cooling applications, making it one of the most explored techniques in this domain. This research paper presents a comprehensive performance evaluation of a latent heat thermal energy storage unit featuring three distinct macro-encapsulation designs for phase change materials. The study aims to assess the thermal performance, efficiency, and practical applicability of these macro-encapsulation designs in a storage system. The PCM macro-encapsulation designs under investigation include cylindrical and rectangular shapes, each possessing different geometry. Two different configurations have been considered in this study. One configuration contains same PCM mass in order to have similar storage capacity while the other configuration has maximum PCM mass that can be inserted inside the tank. The used phase change material is a salt hydrate with melting temperature of 17 °C. The experimental setup consists of a controlled test rig that simulates real-world conditions and enables the comparative analysis of the three designs. Key performance parameters such as the charging and discharging time, temperature profiles, heat transfer rate, and energy storage/retrieval rates are measured and analysed. The results obtained from the experimental study provide valuable insights into the thermal behaviour, energy storage capacity, and overall effectiveness of the three macro-encapsulation designs. It is important to mention that use of an encapsulation design is highly dependent on application. The findings of this study contribute to the understanding of the impact of different macro-encapsulation designs on performance of thermal energy storage units. The results serve as a basis for optimizing macro-encapsulation designs, improving the efficiency and reliability of latent heat storage systems, and promoting their wider adoption in various energy management applications.

1. Introduction

Thermal energy storage (TES) is one of the most promising contemporary technologies which can drive the decarbonization in heating and cooling sector along with increasing the share of renewable energy resources (RES) [1]. TES can be classified in several types e.g., sensible energy storage, latent heat energy storage (LHTES) and thermochemical storage etc. LHTES is one of the extensively researched areas due to its high energy density and the wide range of applications. It employs phase change materials (PCMs) which have the ability to store and release latent heat during phase transitions. The versatility and energy storage capabilities of PCMs make them suitable for various sectors where efficient thermal management and energy storage is essential. Few of the examples can be integration of LHTES with building and HVAC systems [2,3], solar energy systems [4], thermal energy management in industrial processes [5], cold chain and refrigeration systems [6] and thermal management of electronics equipment [7] etc. PCMs are used with the means of micro or macro-encapsulation techniques [8]. Encapsulation of PCM helps to prevent leakage and maintain the stability of the material over time. Encapsulation is mainly distinguished as micro (capsule size ~1–1000 μm) or macro (capsule size above 1000 μm) [9]. Manufacturing of micro-encapsulation involves

* Corresponding author.
E-mail addresses: info@pcmproducts.net (Z. Ure), luisaf.cabeza@udl.cat (L.F. Cabeza).

https://doi.org/10.1016/j.est.2023.109359
Received 3 July 2023; Received in revised form 20 September 2023; Accepted 17 October 2023
Available online 25 October 2023

complex and expensive procedure such as spray drying and interfacial polymerization [10]. On the other hand, manufacturing of macro-encapsulation, which involves enclosing the PCM within larger containers or slabs, requires simple methods which are available at lower costs [11]. Macro-encapsulation provides better protection against PCM leakage compared to micro-encapsulation because of the thicker shell which is less likely to rupture or break, reducing the risk of PCM leakage [12].

The effect of design of macro-encapsulation on thermal behaviour is mainly analysed by numerical analysis in existing literature and few studies have been made experimentally. The literature reviews show that most of the numerical studies performed included spherical and cylindrical modules. A review by Regin et al. [13] reports that only one in over 18 publications used an encapsulation other than spherical or cylindrical. Erlbeck et al. [14] investigated the thermal behaviour of different PCM encapsulations (Cuboid, cylindrical, plate-shaped and spherical) in concrete blocks. The study made use of macro-encapsulated salt hydrate with a meting point of 21 °C in standard shaped concrete blocks for thermal energy storage. Results showed that changing the design of the phase change material encapsulation can affect its thermal behaviour without changing its mass. Different encapsulations provide opportunity to react flexibly to the particular demands and to optimize the thermal behaviour.

Navarro et al. [15] conducted a comparative study on domestic hot water systems using both sensible and latent TES tanks containing PCMs in the form of spheres with a melting point of 58 °C. However, it was observed that the polyethylene balls used as PCM spheres had low thermal conductivity, which negatively affected the reaction time of the latent TES during the charging and discharging processes. Barba and Spiga [16] conducted a study to examine the arrangement of PCM encapsulation and investigated the performance of three PCM shapes (plate, cylinder, and sphere) in the discharge process of a sensible TES tank. The study focused on various factors such as the transient position of the moving surface, temperature distribution, solid PCM quantity, released energy, complete solidification time, the impact of geometry and Jacob number on the final solidification time. The authors determined that the optimal configuration was achieved using small spherical capsules, particularly when a rapid discharge mode is required.

Another such study was carried out by Al-Yasiri and Szabó [17], which investigated the thermal performance of concrete bricks having PCM macro-encapsulated by aluminium containers. The study concluded that encapsulation's surface area is the main parameter in controlling PCM's thermal behaviour provided all PCM capsules have same mass and position. Ismail and Moraes [18] performed a numerical and experimental investigation on solidification of different PCMs encapsulated in cylindrical and spherical shapes of different sizes. All shapes were subjected to similar surface temperature and aim was to find out a suitable pair container-PCM to work efficiently together with refrigeration units. One of the experimental studies carried out with rectangular PCM slabs inside a storage tank by Moreone et al. [2] showed that energy storage capacity of the tank increased by around 35 % when compared with the same tank filled with water. Another study carried out by Heinz and Moser [19] provided insights into a TES system with non-spherical macro-encapsulated PCM. This study contained modelling work for a TES system which produced results quite close to experimental ones. The experimental setup consisted of a TES tank filled with PCM and heat transfer fluid (HTF). Same approach has been used in our study as well. It was observed that storage capacity of tank increased by around 14.5 % with the presence of PCM as compared to tank filled with water only. Vérez et al. [20] performed an experimental study and investigated the thermal behaviour of rectangular slabs which differed in thickness. It was concluded that using thinner slabs helps in achieving higher power and also leads to lower charging and discharging times.

Furthermore, several modelling and simulation studies have been published on use of PCM in buildings for cooling applications. One such example is of study performed by Faraj et al. [21] in which different TES systems containing PCMs were studied for cooling applications in buildings. It was concluded that incorporating PCM is a potential technique for creating energy-efficient buildings. Moreover, it was also speculated that bringing together active and passive systems might be a step towards net zero energy buildings. Another review study conducted by Liu et al. [10] provides insights into PCM melting processes and material selection at the component level as well as ideal placements at the system level.

Following studies highlight the importance of PCM macro-encapsulation designs, configurations and their impact on heat transfer rates. Dallaire et al. [22] investigated a study on dual-stack latent heat thermal energy storage (LHTES) through experiments for cooling applications in buildings. It was concluded that tested system can be successfully integrated with commercial ventilation systems. Another study performed by Zhang et al. [23] investigated the fin designs to optimize the heat transfer performance of LHTES. The designs which were thoroughly reviewed are helical, longitudinal, topology optimized (termed as most advanced fin design methodology), annular and multiple-finned tubes. Another such study by Oliveski et al. [24] investigated design of fin structures for PCM melting process in rectangular activities. An optimized aspect ratio of fin was figured out while keeping the mass constant. Another study carried out by Dong et al. [25] investigated heat transfer and phase transition in PCM balls inside cold storage tank. It was reported that while keeping the same velocity of cooling water, freezing rate of PCM spheres increased with smaller diameter. Another study performed by Sharma et al. [26] sheds light on solidification of nano-particle-based PCM in a fin-aided triplex-tube energy storage system. This study was also aimed at cooling applications and investigated different volume concentrations of copper oxide particles on attached and detached fins. Ding et al. [27] performed analysis of a 20-feet LHTES device integrated with a building for cooling purposes. A novel fin plate was designed in order to increase the heat transfer rate of PCM for restricted charging process. The use of straight fin resulted in higher heat transfer rate as compared to branched fin. A study by Bejarano et al. [28] modelled a novel scheme for a LHTES system for cooling application. The objective of the study is to store and release energy generated by refrigeration cycle. Two dynamic models are developed namely continuous and discrete to study the charge and discharge process. A mathematical model was developed by Anand et al. [29] to improve the performance of a PCM cold box using two bilayers configurations. It was reported that double bilayer configuration performed better than single bilayer and thus the storage time of frozen materials inside PCM cold box is increased by 30 %. Another such study which investigates the energy release of a LHTES system with multiple PCMs is performed by Mehalaine and Lafri [30]. It was concluded that triangular cross-section cells increase solidification and complete energy discharge durations by around 42 % and 25 %, respectively, while also enhancing convection. The performance of energy charging is also improved by around 40 %. Bianco et al. [31] made a study on multi-objective optimization of a PCM based heat exchanger for cold thermal energy storage. The storage unit was both experimentally and numerically analysed. Charging and discharging times were optimized using multi-objective genetic algorithm. The novel algorithm helped in exploiting 72 % of stored latent heat. Soh et al. [32] did design optimization of a low temperature LHTES unit for cooling applications at system level. It was observed that the main factor influencing discharge efficiency is thermal stratification. Moreover, the proposed scheme helped in improving charged cold energy for the same duration by 54.7 % when compared with a previous study.

Most of the above-mentioned studies are based on numerical simulations and few of the experimental studies focus only on single configuration. Furthermore, the studies involving the optimisation of system are referring to two aspects e.g., fin design to enhance heat transfer rate and inlet velocity of heat transfer fluid. Some of the studies investigated multi-layered PCM configurations but they are also numerical based studies. Few examples of systematic optimization of PCM

configurations exists which are however based on numerical simulations. To the best of authors' knowledge, no study is available on comparison of different commercial macro-encapsulation designs in which PCM behaviour is also assessed in addition to that of the PCM tank as a whole.

This study discusses the role of macro-encapsulated PCM for cooling applications. There can be several cooling applications that can be served with a PCM storage having melting point around 17 °C. One such example is wine cellars where wine storage requires specific temperature conditions to preserve the quality of the wine [33]. For many types of wine, a temperature of around 17 °C is considered optimal to slow down the aging process and allowing the wine to mature properly. Moreover, artwork and historical artefacts often require controlled environments to prevent damage due to temperature fluctuations [34]. Maintaining a consistent temperature of around 17 °C helps to preserve delicate materials, such as paintings, sculptures, and manuscripts, ensuring their longevity. Furthermore, data centres house computer servers and other equipment that generate a significant amount of heat. Maintaining a temperature around 17 °C helps to prevent overheating and ensures the proper functioning of the servers, reducing the risk of damage and data loss [35]. Other applications may include scientific laboratories which require precise temperature control and deal with sensitive materials, chemicals, or biological samples that may require a stable temperature of 17 °C to maintain sample integrity and ensure accurate results. Food storages and greenhouses can be the other examples of employing such cold storage [36,37]. Such a storage design can also be integrated with a heat pump to pre-heat the water or air in colder climates. Moreover, it can also be used for high temperature cooling or low temperature heating applications [38].

In this paper, for the first time, thermal behaviour of a commercial thermal energy storage (TES) tank for cold applications is analysed experimentally using three different commercial macro-encapsulation designs, namely TubeICE, ThinICE, and FlatICE. TubeICE is cylindrical in shape while other two encapsulations are rectangular slabs with difference in thickness. Performance of TES unit is analysed in terms of storage capacity, heat transfer rate profiles and temperature distribution inside the tank. The novelty of paper lies in comparing different macro-encapsulation designs and providing insights on state of charge (SoC) of TES unit along with time and energy which can be useful for future control implementations for TES tanks. Furthermore, details are also provided on energy storage density, and charging and discharging powers for different encapsulation designs. Two experimental configurations are proposed with different arrangement of PCM capsules inside the tank which will help to understand the role of encapsulation designs in a better way. The PCM used is PlusICE 17 which is a salt hydrate. The comparison of results is made in terms of energy efficiency and energy density for all encapsulation designs. Results obtained from this activity will be beneficial for industry related with TES energy systems to optimize future designs of TES storage tanks as well as encapsulation designs.

2. Materials and methods

2.1. Materials

PlusICE S17 (salt hydrate), a commercial product of PCM products [39], is used for this scientific study. Thermal properties of PlusICE S17 are given below in Table 1. For all the analyses and calculations, the properties provided by the supplier were used.

Three different macro-encapsulation designs namely ThinICE, TubeICE and FlatICE have been experimentally tested. These encapsulations are shown in Fig. 1.

The dimensions for each encapsulation are given below in Fig. 2. ThinICE and FlatICE are similar in length and width and differ in thickness. Moreover, the spacing between two consecutive capsules is higher for ThinICE as compared to FlatICE which means more HTF channels will be available for ThinICE. FlatICE has twice the thickness of ThinICE. Lowest thickness of ThinICE resulted in allowing more slabs inside the tank as compared to FlatICE. TubeICE has a length of 1200 mm while diameter is 50 mm.

Table 1
Thermal properties of PCM [40].

Properties	Values
Melting temperature (°C)	17
Density (kg/m^3)	1525
Latent heat capacity (kJ/kg)	155
Specific heat capacity (kJ/kg·K)	1.9
Thermal conductivity (W/m·K)	0.43
Maximum operating temperature (°C)	60

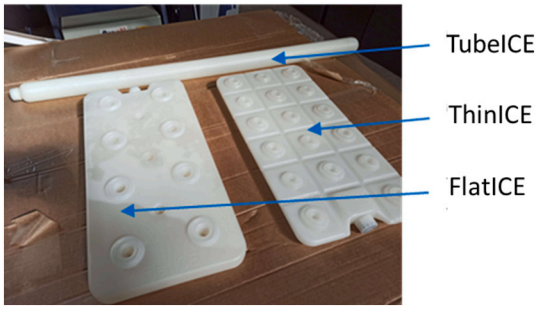

Fig. 1. Three macro-encapsulation designs.

2.2. Experimental setup

Experiments were carried out in a research facility at GREiA research group in University of Lleida. The experimental setup, shown in Fig. 3, can be used to perform tests on LHTES for low to medium temperature range applications (−20 °C < T < 100 °C). The t experimental setup is described in details in [20].

The system consists of a TES tank, two variable speed pumps to regulate the inlet temperature and mass flow rate of the TES tank and a flowmeter Badger meter type ModMAG M1000. An inertial tank, containing 200 l of water, permits the charging and discharging operations of the TES tank. Its temperature is controlled by a chiller and two immersion thermostats of 3 kW power each. The chiller is of Zanotti model GCU2030ED01B and has a cooling capacity of 5 kW [41]. The immersion heaters are electrical resistances from Asturgo model RIA-207 [42]. The components are connected together through copper pipes of 0.5″ diameter. The pipes are insulated with 18 × 0.9 mm polyurethane tubes. The data acquisition system consists of data logger, a computer and data acquisition software SCADA which is developed in Indu Soft Web Studio [43]. The data logger used is 3 STEP DL-01 [44].

The temperature inside the TES tank is maintained through the water inertia tank. For charging the TES tank, temperature inside the inertia tank is increased through immersion heaters. For discharging process, temperature is cooled down using a chiller. The speeds of two pumps are controlled to keep temperature and mass flow rate constant at inlet of TES tank. The commercial tank used for this scientific study has a volume around 490 l.

The details of TES tank used for experiments is shown below in Fig. 4. A diffuser is used to distribute the water flow uniformly. After putting all the encapsulations inside tank, it is closed with a lid from top. Fig. 4 (a) shows the dimensions and process of filling up the tank with encapsulations while Fig. 4 (b) shows the tank filled with encapsulations and water.

The temperature is measured using 27 thermocouples which are pasted on top of encapsulations with silicon glue. The thermocouples used are shown in Table 2 below. Class B thermocouples are used for

Type of Slab	A	B	C	D	E	F
ThinICE	250	500	17	16	10	6
FlatICE	250	500	35	10	7	3
TubeICE	1200	50				

dimensions in millimetres

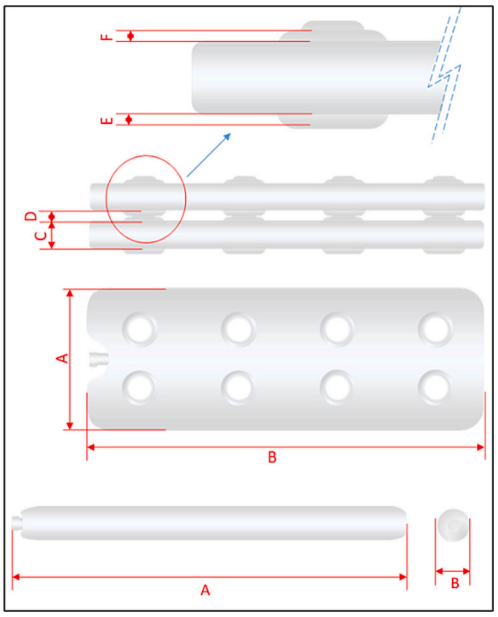

Fig. 2. Dimensions of macro-encapsulations.

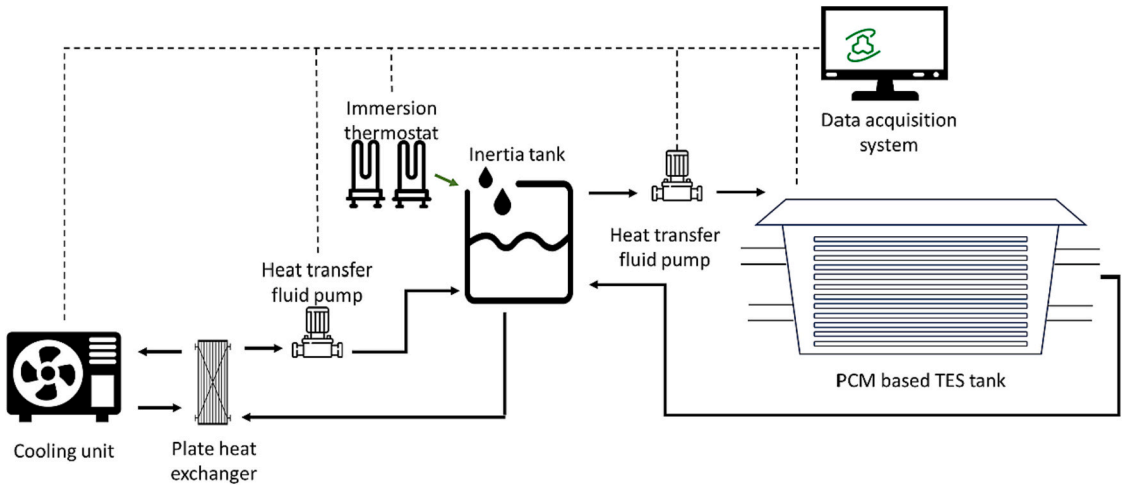

Fig. 3. Schematic diagram of experimental setup [20].

measuring PCM temperature while six class A thermocouples are used for measuring HTF fluid temperature at the inlet and outlet of tank.

The sensors are fixed at the external surface of capsules at different heights: 400 mm (TOP), 260 mm (MID) and 110 mm (BOTTOM). The schematic diagram of sensors positioning is shown in Fig. 5.The red dots represent the positions of sensors. These sensors were named as T1, T2, T3 and so on.

2.3. Heat loss test

An important aspect of a system performance is heat loss characteristics of storage. It is represented using average heat loss coefficient or U-value, which overlook the intricate geometry of thermal storage and the effects of inlet and outlet ports that can act as thermal conduits [45]. A heat loss test was carried out to analyse the heat loss through the tank. For this purpose, water was circulated at 7 °C until HTF and PCM maintains a temperature of 7 °C and then tank was exposed to ambient temperature. Test was considered complete when all sensors attained the value of 27 °C. The U value of the tank came out to be 2.1 $W/m^2{\cdot}K$. Heat losses are considered in the calculations (equation provided in Appendix). The obtained U value is compared with the U values of commercially available tanks in literature. A study carried out by Vérez et al. [46] reported U values for top, lateral and bottom sides of a 0.54 m^3 vacuum insulated tank as 0.32, 0.38 and 2.00 $W/m^2{\cdot}K$. Another study carried out by Cruickshank et al. [45] calculated U value of a 0.27 m^3 commercial water tank insulated with fibre glass. The U values reported for top lateral and bottom sides of tank were 0.66, 1.05 and 2.54 $W/m^2{\cdot}K$.

Heat loss test points out that losses are higher than expected. Shape factor is of little importance here and a better insulation is required for commercial applications.

2.4. Methodology

The temperature for charging and discharging of PCM tank was taken as 27 °C and 7 °C which is ±10 °C of melting point of PCM i.e., 17 °C. The flow rate was 0.07 kg/s and it was kept constant for all experiments. A summary of all the parameters including temperature and mass flow rate is shown in Table 3.

To perform a charging process, the PCM in the tank was cooled down

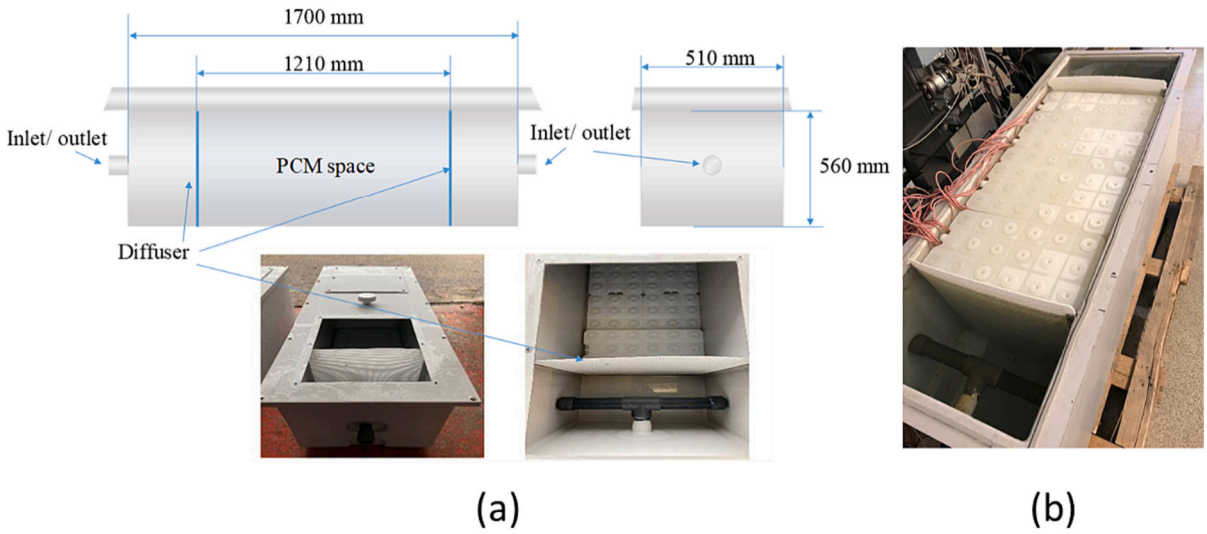

Fig. 4. Latent thermal energy storage tank. (a) Dimensions, (b) full view.

Table 2
Uncertainties of parameters involved in this study.

Parameter	Units	Sensor	Accuracy
Temperature	°C	Pt-100 1/5 DIN class B IEC 60751	$\pm 0.3 + 0.005 \cdot T$
Temperature	°C	Pt-100 1/5 DIN class B IEC 60751	$\pm 0.15 + 0.002 \cdot T$
Flow rate	L/min	Badger meter type ModMAG M1000	±0.25 %

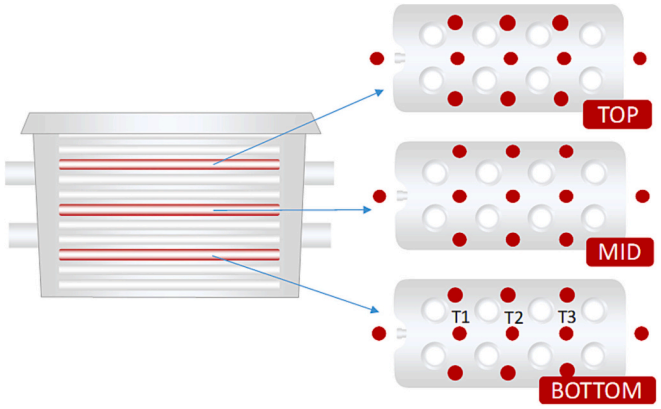

Fig. 5. Positioning of thermal sensors within the storage tank.

Table 3
Experimental boundary conditions.

Variable	Charging	Discharging	Selection criteria
Initial tank temperature [°C]	7	27	± 10 °C from the phase change temperature (27)
Final tank temperature [°C]	27	7	± 10 °C from the phase change temperature (27)
Flow rate [kg/s]	0.07	0.07	–

until all the sensors indicated a value of 7 °C ± 1 °C and then HTF temperature was set at 27 °C and flow rate to 4 l/min at tank inlet. Experiment was considered complete when all PCM sensors inside tank reached a temperature in the range of 27 °C ± 1 °C. To perform a discharging process, the tank was first brought to a temperature of 27 °C and then HTF was circulated at 7 °C. The experiment was considered complete once all PCM sensors inside tank reached a temperature in the range of 7 °C ± 1 °C. At least three repetitions of all the charging and discharging experiments were done for all three encapsulations.

2.5. PCM storage design layouts

The PCM encapsulation can have different configurations inside the tank. In this study, two configurations were tested. One of these configurations contained equal PCM mass inside the tank, for all encapsulations, to ensure similar storage capacity. The other configuration contained maximum amount of PCM mass that can be put inside the tank with three encapsulations. These two configurations were tested to analyse the thermal behaviour of encapsulations and also to see if one configuration has any advantage over the other. ThinICE encapsulation was taken as a reference for both configurations.

2.5.1. Layout 1: similar storage capacity

Layout 1 contained the equal amount of mass of PCM inside the tank for all three encapsulations in order to have similar storage capacity. To ensure uniform distribution of PCM capsules inside tank, spacers were used for TubeICE and FlatICE. The spacers are shown in Fig. 6.

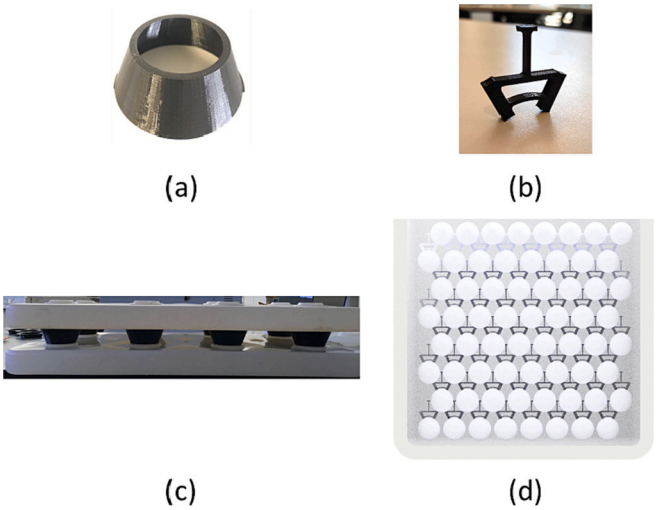

Fig. 6. (a) Spacer for FlatICE, (b) spacer for TubeICE, (c) tank configuration with spacers for FlatICE, and (d) tank configuration with spacers for TubeICE.

2.5.2. Layout 2: maximum packing factor

The second layout for carrying out experiments had the maximum volume of PCM that could fit inside the tank. So, in the second category, experiments were carried out with maximum packing factor. The above-mentioned experimental layouts will be referred to as layout 1 and layout 2 hence forthwith.

The Tables 4 and 5 contain information about the number of capsules to be put inside the tank and their distribution, total PCM mass and theoretical stored energy. Equations used are shown in Appendix section.

2.6. Data analysis

The data recording interval was set to 1 s. The data was obtained and calculations involving heat losses were made. For these calculations, the log mean temperature difference method was used. Furthermore, averages of sensors at top, middle, and bottom levels of PCM encapsulation and HTF were taken and used for further analysis. Eventually, power and energy calculations were carried out. The equations used for these calculations are shown in Appendix section.

3. Results and discussion

3.1. Results for experimental layout 1: similar storage capacity

3.1.1. Charging process

The temperatures presented herein represent the average values of PCM and HTF temperatures. These averages were obtained from a comprehensive array of thermocouples, consisting of 27 sensors distributed across the surface of the slabs and 6 sensors placed within the HTF channels. Fig. 7 illustrates the temporal temperature profiles for three different encapsulations with similar storage capacities. The temperature of HTF for three macro-encapsulation designs is presented on secondary vertical axis while primary axis contains PCM temperature. Upon analysing the average PCM temperature (referred to as T_PCM_avg_encapsulation name in the figure), it was observed that FlatICE and TubeICE exhibited faster charging rates compared to ThinICE which required a longer duration to attain full charging conditions. Furthermore, Fig. 8 demonstrates that ThinICE exhibited a substantial temperature gradient of up to 7 K between the upper and lower HTF layers. This gradient resulted in a prolonged charging time for the lower section of the tank due to the accumulation of colder water at the bottom, owing to its higher density. The temperature gradient was calculated as the difference between the uppermost and lowermost temperature sensors in the tank. TubeICE initially exhibited a high temperature gradient, which gradually diminished over time.

The HTF fluid channels are quite wide for TubeICE and FlatICE since spacers have been used for uniform distribution of PCM mass inside the tank to ensure similar storage capacity. Specifically, the HTF channels in ThinICE have a width of 16 mm, while in FlatICE, the channels are 24 mm wide. The precise dimensions of the HTF channels in TubeICE are challenging to ascertain due to the unique shape of the spacers. However, it is evident that the cross-sectional area of the HTF channels in TubeICE exceeds that of ThinICE. Unlike ThinICE's and FlatICE's HTF channels, which have a rectangular shape, TubeICE's channels have an irregular shape. Consequently, the HTF fluid flows not only through the specially designed spacers but also through the gaps present between the cylindrical capsules.

In order to assess the fluid flow characteristics, the Reynolds number (Re) is employed as a dimensionless parameter to determine the flow regime, whether it is laminar or turbulent. Calculations conducted for the *Re* number indicate that the flow within the HTF channels of all three encapsulation systems is laminar. For FlatICE, the *Re* number is determined to be 1860, while for ThinICE, it is 670. Due to the unique shape of TubeICE spacers, obtaining an accurate value for the *Re* number is challenging. However, based on Fig. 7, which illustrates the lower charging time of TubeICE compared to ThinICE, it can be inferred that the *Re* number for TubeICE is significantly higher than that of ThinICE. The larger HTF channels in TubeICE result in a greater hydraulic diameter and higher velocities, contributing to higher *Re* numbers. Conversely, lower *Re* numbers are associated with thicker boundary layers, which lead to less efficient heat transfer. Consequently, ThinICE requires more time to complete the charging process.

Table 4
Experiment layout 1 (similar storage capacity).

Encapsulation	No. of slabs	PCM mass (kg)	Distribution		Theoretical energy stored (kWh)
			Rows	Columns	
ThinICE	64	156	16	4	16.5
TubeICE	64	157.4	8	8	16.2
FlatICE	34	155	8.5	4	16.9

Table 5
Experiment layout 2 (maximum packing factor).

Encapsulation	No. of slabs	PCM mass (kg)	Distribution		Theoretical energy stored (kWh)
			Rows	Columns	
ThinICE	64	156	16	4	16.5
TubeICE	124	305	12.4	10	20.8
FlatICE	52	260	13	4	19.9

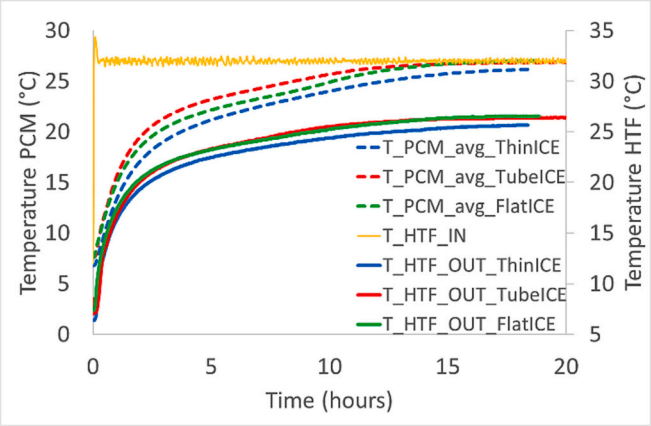

Fig. 7. Charging temperature profile for three encapsulations.

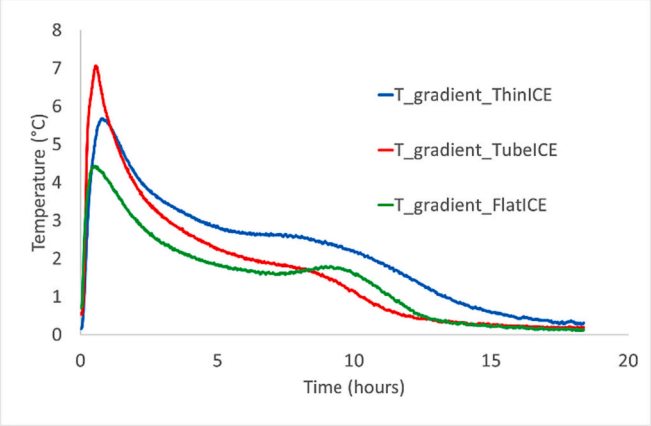

Fig. 8. Temperature gradient between upper and lower HTF layer for three encapsulations.

TubeICE and FlatICE comprise eight and nine HTF channels, respectively, whereas ThinICE incorporates sixteen channels. The velocity of the HTF is distributed among the consecutive channels, and a higher number of channels with smaller hydraulic diameters result in reduced velocities. This, in turn, yields lower *Re* numbers and less efficient heat transfer. This discrepancy could be one of the factors contributing to the higher temperature gradient observed in ThinICE compared to the other two encapsulation designs. To accommodate the higher temperature gradient, ThinICE necessitates additional time, thereby prolonging the charging duration.

Fig. 9 represents the charging power profile for all three encapsulations for similar storage capacity. Due to characteristics of experimental facility, the inlet HTF temperature oscillates by ±2 °C around the required temperature but later it become stable before the HTF temperature inside the tank reaches the latent range of PCM. Power profile showed an exponential trend with a higher slope in first 2 h. During this time, heat is mainly being supplied to HTF inside the tank and thus higher temperature gradient results in higher heat transfer rate. As the temperature gradient between HTF inlet and tank temperature decreases, the power curve starts to decrease. Charging power for TubeICE drops quite sharply with the passage of time as temperature gradient decreases quite fast. ThinICE provides a higher power for a longer period as compared to other encapsulations.

3.1.2. Discharging process

Fig. 10 represents the temperature profiles for discharging process for three encapsulations. During discharging process, the PCM temperature of FlatICE took the longest time to get discharged completely followed by ThinICE and TubeICE respectively. The HTF temperature dropped quite sharply for FlatICE in first hour and then got stable. ThinICE and FlatICE return quite similar profiles for HTF temperature after 5 h of discharging process. The PCM effect can be seen in the enlarged version of graph. The FlatICE configuration exhibited a considerable delay in reaching the discharging state of the PCM temperature. One potential explanation for this behaviour is the larger width of the FlatICE capsules, which is twice that of ThinICE. Consequently, during the discharging process, where conduction plays a dominant role, the rate of heat exchange within the PCM diminishes. This reduction in heat exchange rate leads to an extended duration required to reach the discharging state.

Fig. 11 represents the discharging power evolution of three encapsulations for discharging process. The discharging power profiles exhibited an exponential trend, with TubeICE demonstrating higher power delivery during the first hour. The power values for FlatICE were lower during the initial 4 h but subsequently increased during the latter half of the discharging process. The divergence in the initial power values can be attributed to the oscillating nature of the tank inlet temperature at the outset. However, it is worth noting that the temperature became stable well before the latent phase commenced within the tank.

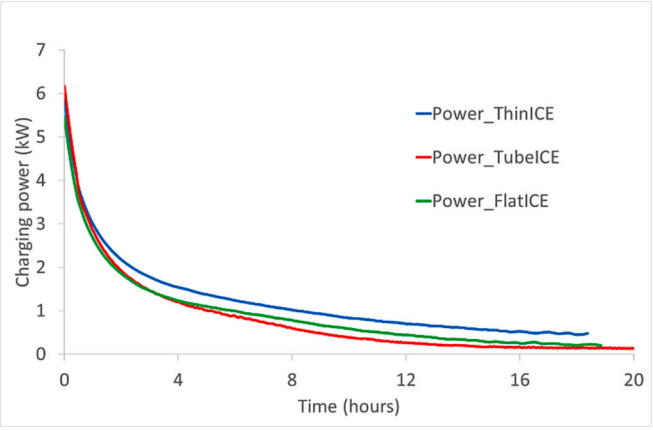

Fig. 9. Charging power profile for three encapsulations.

3.1.3. Stored and released energy

Fig. 12 shows the energy delivered to the PCM storage tank during charging process of three presented cases. The discrepancy in the values of stored energy falls within the range of measurement uncertainty. Additionally, the end of a discharging experiment was regarded as the starting point of a subsequent charging experiment. However, it should be noted that the electrical resistances required some time to raise the temperature of the inertia tank from 7 °C to 27 °C. During this interval, heat losses occurred, causing a decrease in the temperature within the tank. This variation in temperature can be one of the contributing factors leading to differences in the stored energy, despite having the same PCM mass. FlatICE was able to recover 84 % of the stored energy while ThinICE and TubeICE managed to recover 80 % of the stored energy as also shown in Table 7. TubeICE takes somewhere around 12 h to release the above-mentioned amount of energy while both ThinICE and FlatICE require around 15 h to release the abovementioned amounts of energies. So, for applications needing the release of energy in a relatively shorter period of time, TubeICE is suitable option while for applications needing stable release of energy for a longer period of time can employ ThinICE and FlatICE.

The presence of latent storage in ThinICE, TubeICE, and FlatICE proved beneficial in terms of storing and releasing higher amounts of energy compared to sensible thermal energy storage (TES). Specifically, these encapsulation systems were capable of storing approximately 48 %, 41 %, and 45 % more energy, respectively, when compared to an equivalent volume of sensible storage (approximately 490 l) with a temperature difference of 20 K.

Regarding energy discharge, the TES tank exhibited a higher energy delivery capacity. For ThinICE and FlatICE, the TES tank was able to deliver around 20 % more energy, while for TubeICE, it provided approximately 12 % more energy, compared to a similar volume of sensible TES. This highlights the advantages of utilizing latent storage systems, as they offer enhanced energy storage and release capabilities when compared to their sensible TES counterparts.

Fig. 13 represents the time variation needed to increase 5 % of the energy accumulated in PCM tank. It provides a detailed profile time study for charging process. These details can help in various control applications involving TES. If a TES tank is needed to be used for partial load conditions, the detailed profile time study will help to develop a suitable control. Results show that the time variation to store an increased amount of energy increases as the charging process proceeds since temperature gradient between PCM and HTF reduces. To store the last 5 % of accumulated energy, all encapsulations took a lot longer because of low temperature gradient. Gasia et al. [47] used the same methodology to show the detailed profile of a latent thermal energy storage unit. The black dashed line represents the accumulated time value. The y-axis is in logarithmic scale. For all three cases, energy accumulation rate is quite high initially which becomes slower in the middle of process and then eventually becomes almost stagnant. The reason is that initially, major portion of the heat is transferred to the HTF inside tank and later this heat is transferred to PCM capsules too which slows down the process. Furthermore, higher temperature gradient initially between HTF inlet and PCM inside the tank results in higher heat transfer rates and later drops down as temperature difference reduces. Moreover, ThinICE stored almost 90 % of total stored energy in 60 % of the total process time while TubeICE and FlatICE took 54 % and 56 %, respectively. Furthermore, another important information that can be extracted from is that ThinICE accumulates 90 % of the total energy almost 13 % and 20 % faster than the TubeICE and FlatICE, respectively.

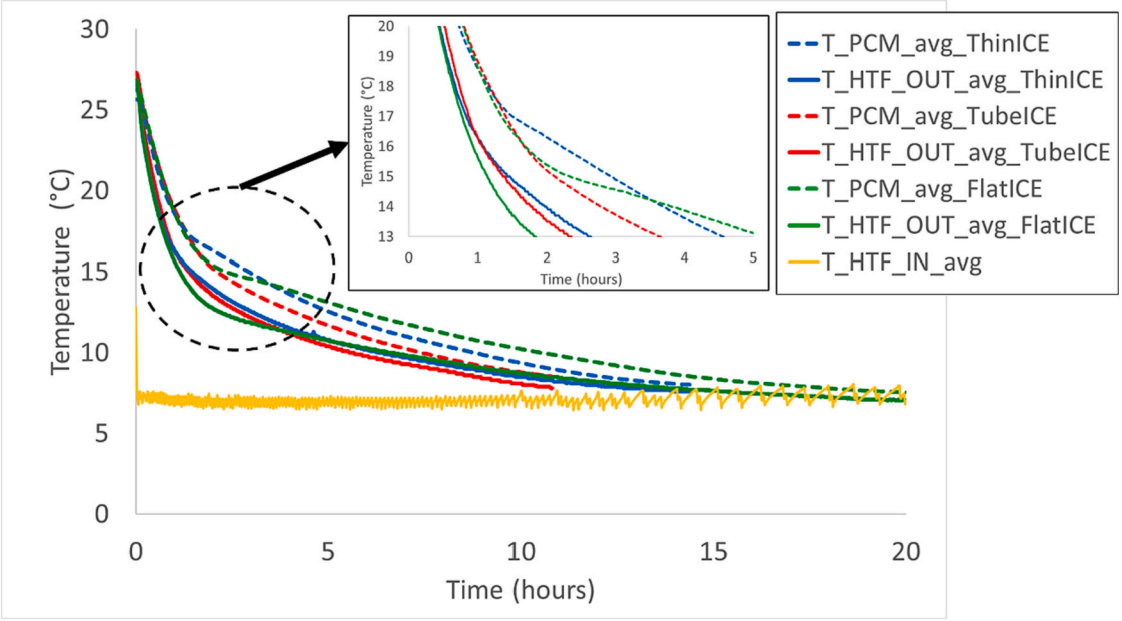

Fig. 10. Discharging temperature profile for three encapsulation systems.

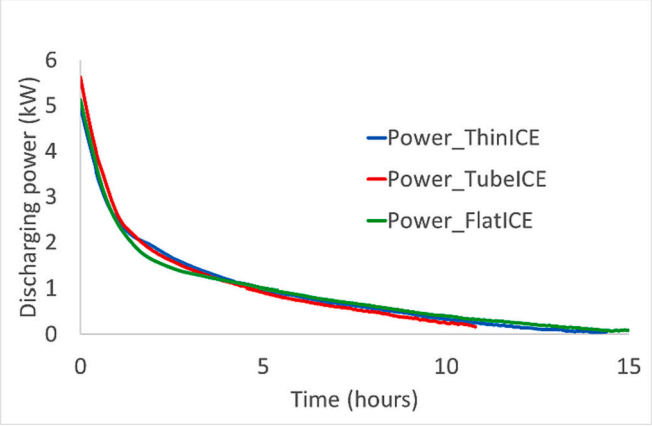

Fig. 11. Discharging power profile for three encapsulation systems.

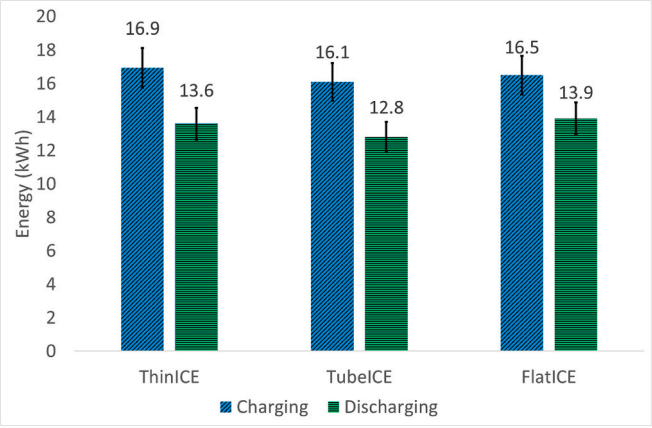

Fig. 12. Total energy stored and discharged for three encapsulation systems.

3.2. Results for experimental layout 2: maximum packing factor

3.2.1. Charging process

Fig. 14 contains the temperature curve for all encapsulations for charging process. ThinICE takes shortest time to get charged mainly because of 40 % and 49 % less PCM mass as compared to FlatICE and TubeICE respectively. In first 2 h, both TubeICE and FlatICE show the same trajectory but later the average HTF outlet temperature for FlatICE decreases because of stratification effect. Although a constant stratification profile has been achieved for all encapsulation systems but this effect is more visible in FlatICE where the lower part of the tank takes longer time to get charged. Tank with FlatICE offers smaller HTF channels as compared to other configurations which results in higher opposition to HTF flow. This opposition enhances the flow distribution of HTF towards upper and middle regions of tank which have relatively similar density as HTF inlet one. In this configuration, FlatICE has HTF channels as wide as 10 mm while ThinICE has 16 mm wide channels. ThinICE has a higher *Re* number value i.e. 670 as compared to FlatICE which is 530. For TubeICE, it is difficult to approximate the dimensions of HTF channels and thus the value of *Re* number.

Fig. 15 represents the charging power during charging process for three encapsulation systems. ThinICE exhibits a higher power output during the initial stage of charging, whereas both FlatICE and TubeICE configurations deliver similar power levels. The charging power for ThinICE is initially higher during the first 2 h but gradually decreases over time. In contrast, FlatICE demonstrates a power output that closely matches that of the TubeICE configuration for the majority of the charging process, but then experiences an increase in power output later on.

3.2.2. Discharging process

Fig. 16 represents discharging temperature profile for average PCM and HTF outlet temperature. Analysing the results obtained, ThinICE finished discharging process almost 13 % faster than FlatICE and TubeICE owing to the less amount of PCM. Upon discharging, TubeICE showed stratification effect which became more pronounced and obvious as the discharging process progressed with time. Moreover, the temperature for TubeICE dropped quite sharply only to become stable with time. FlatICE and TubeICE had similar HTF profile after 5 h of discharging process while average PCM temperature profile was

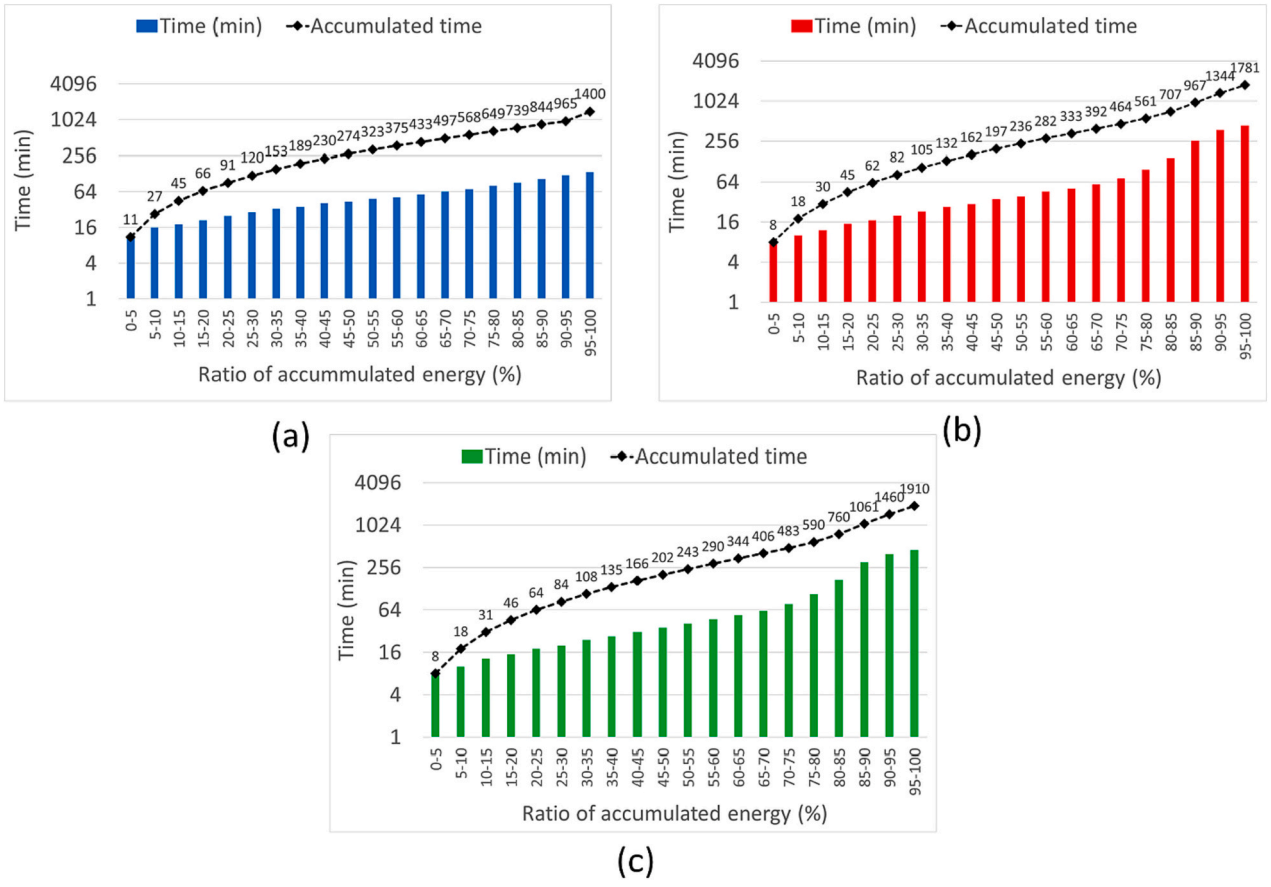

Fig. 13. Ratio of accumulated energy (%) (in bars) in terms of time (accumulated time in dashed line) with (a) ThinICE, (b) TubeICE, and (c) FlatICE.

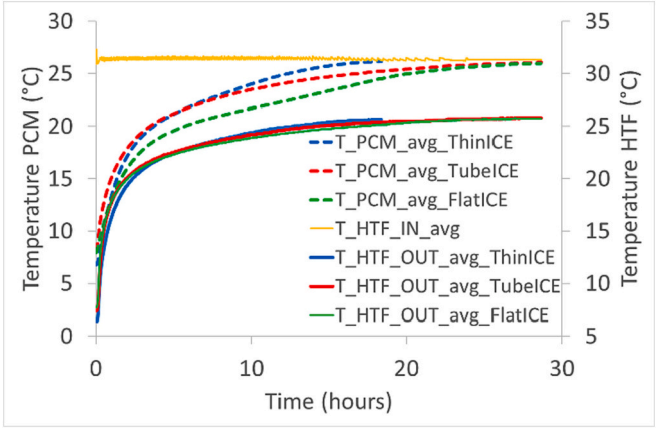

Fig. 14. Charging temperature profile for three encapsulation systems.

different from each other.

The discharging power evolution during discharging process for three experiments is shown in Fig. 17. An exponential trend was achieved for power evolution with significantly higher values in first hour. This oscillation of temperature affects the initial peak obtained for all three encapsulations. ThinICE finishes the discharging process earlier than other two encapsulations mainly because of less PCM mass inside tank. TubeICE initially returns lower value for power but later it becomes stable. For first 2 h, ThinICE and FlatICE show a similar trend for charging power but later the power for FlatICE increases.

3.2.3. Stored and released energy

Fig. 18 reports the energy stored and released for each encapsulation type. FlatICE was able to store highest amount of energy among three encapsulations followed by TubeICE and ThinICE. It stored 8.4 % and 22.5 % more energy than TubeICE and ThinICE respectively. When it comes to energy released, as shown in Table 7, TubeICE managed to deliver around 82 % of the stored thermal energy. ThinICE delivered around 81 % while FlatICE managed to recover around 78 % of stored thermal energy. Considering the range of uncertainty measures, the storage efficiencies of all three encapsulations are quite close to each other. From applications point of view, rate of energy recovery is an important factor along with amount of energy released. In terms of rate of energy recovery, ThinICE delivered around 85 % of energy stored by FlatICE and TubeICE 13 % faster than other two encapsulation systems.

If the values for energy stored and released for two configurations are compared, FlatICE in layout 1 discharged 86 % of the energy, that too 25 % faster, delivered by FlatICE in layout 2. Moreover, TubeICE in layout 1 managed to discharge around 82 % energy of energy delivered by TubeICE in layout 2 while being 40 % faster. ThinICE was considered as a reference for these two sets of experiments, so values obtained are similar for both layouts. The obtained results indicate that Layout 1 is more favorable in terms of achieving expedited heat exchange.

Fig. 19 shows the ratio of accumulated energy in percentage for experimental layout 2. ThinICE accumulates 90 % of the energy in 60 % of total process time while TubeICE and FlatICE take 63 % and 69 % of total process time. This implies that in order to reach 90 % of storable energy for each encapsulation type, ThinICE encapsulation is the fastest to reach this level and takes 23 % and 34 % less time than TubeICE and FlatICE, respectively.

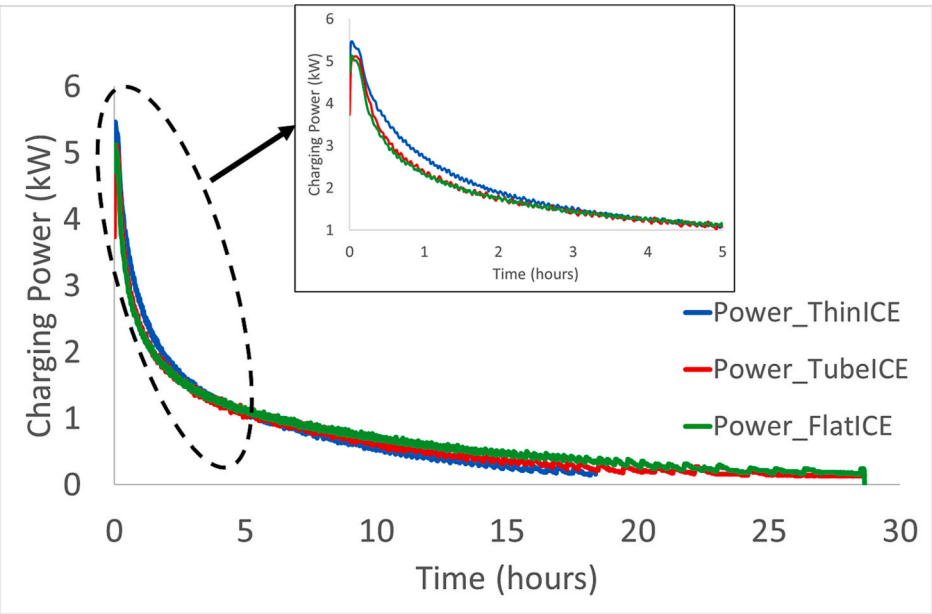

Fig. 15. Charging power profile for three encapsulation systems.

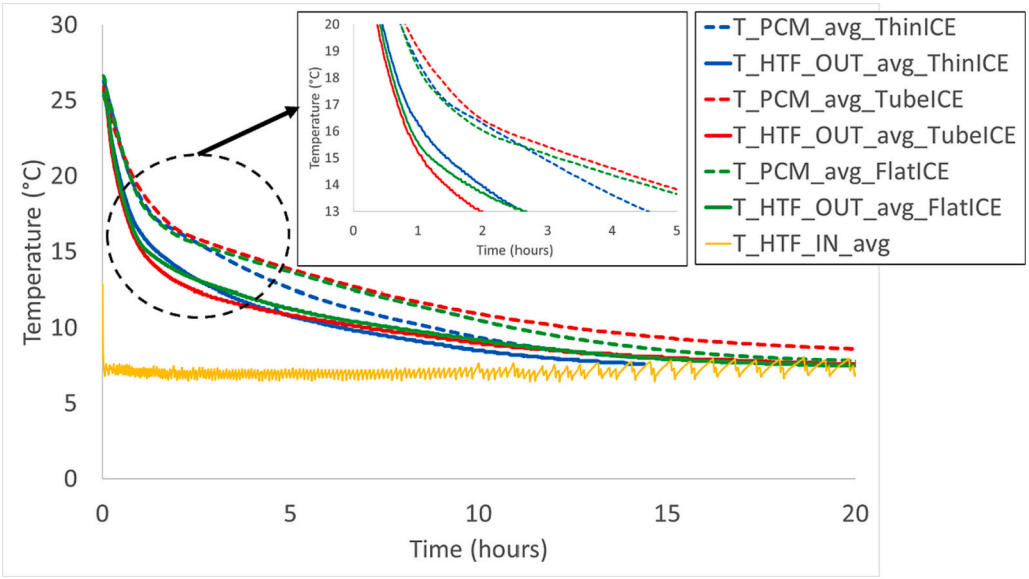

Fig. 16. Discharging temperature profile for three encapsulation systems.

4. Discussion

4.1. Effectiveness of the latent TES

The results obtained during the experimental campaign were further analysed with a twofold scope: retrieving engineering information on the layouts tested, which can be useful for further design improvement, and compare the obtained results with previous works related to the use of PCM tanks in combination with HVAC systems. To this aim, a methodology well established in the literature was used, which is based on the calculation of the performance of the tank extending the epsilon-NTU method for heat exchangers.

The performance of a heat exchanger is defined through heat exchange effectiveness. It can be argued that a TES device with incorporation of PCM is a heat exchanger as mentioned by Sari and Kaygusuz [48]. The effectiveness of a heat exchanger is a measure of its ability to transfer heat between two fluids. It is defined as the ratio of the actual heat transfer to the maximum possible heat transfer between the two fluids. In other words, it indicates how efficiently the heat exchanger is performing its function. Eq. (1) represents the instantaneous effectiveness during the process while Eq. (2) represents the average effectiveness of whole process. T_{in}, T_{out} represent the tank inlet and outlet temperatures while T_{PCM} represents the temperature of PCM. This methodology was adopted by Tay et al. [49] to determine effectiveness of tube-in-tank phase change TES systems. These equations for effectiveness can be used for all kinds of PCM systems including tubes, plates and spheres inside TES tank [49]. Effectiveness will be higher when T_{PCM} will approach the T_{out}.

$$\varepsilon = \frac{(T_{in} - T_{out})}{(T_{in} - T_{PCM})} \tag{1}$$

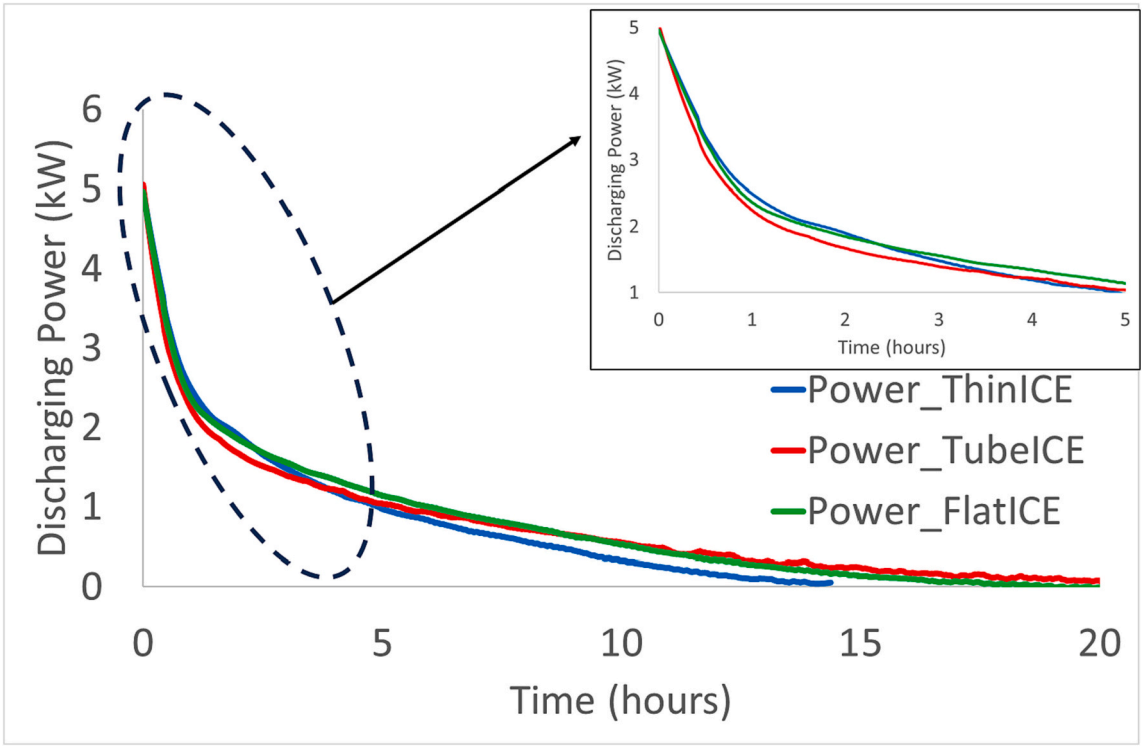

Fig. 17. Discharging power profile for three encapsulation systems.

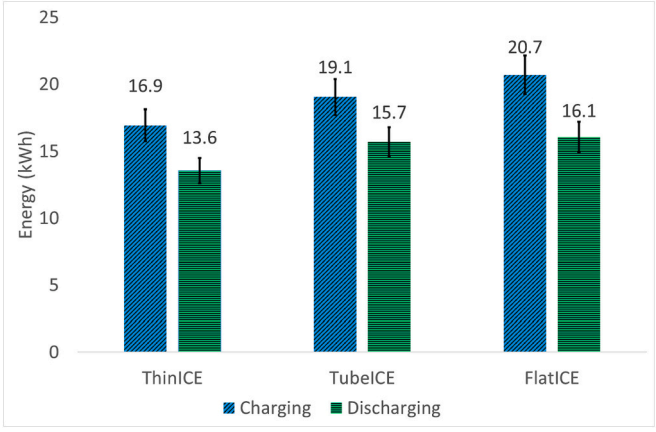

Fig. 18. Total energy stored and discharged for three encapsulation systems.

$$\bar{\varepsilon} = \int_0^t \varepsilon \, dt \tag{2}$$

Table 6 contains results for charging effectiveness of three encapsulations for both layouts. TubeICE reported highest effectiveness value for layout 1 while ThinICE reported highest effectiveness value for layout 2. The results suggest that for TubeICE and FlatICE, charging effectiveness has reduced for layout 2. These encapsulations reported high effectiveness values for layout 1 since HTF channels are wider because of presence of spacers. In layout 2, HTF channels are narrower and thus it altered the effectiveness. Wider channels resulted in higher *Re* number and thus higher effectiveness. One reason of ThinICE having high effectiveness value lies in the smaller thickness of capsule. Lower the thickness, higher will be the heat transfer rate. In order to have higher effectiveness and faster heat exchange, use of layout 1 is recommended.

The values of effectiveness obtained are compared with the values available in literature. A study carried out by Aziz et al. [50] used effectiveness-NTU method to optimize a packed bed PCM of spherical capsules. Twenty different TES configurations were analysed using above mentioned method. In this study, mass flow rate was varied and charging effectiveness was calculated accordingly. It was observed that effectiveness decreased with increasing mass flow rate. The configuration with nearly constant compactness factor with various radius values had effectiveness as high as 0.9 and as low as 0.2. The other configuration with fixed radius and various lengths had effectiveness in the range of 0.75 to 0.95. Further details can be found in the reference [50]. Another study by Tay et al. [49] also used the same method to find effectiveness of a tube in tank LHTES system. Effectiveness was plotted against mass flux for different number of tubes in tank. For a single tube in tank configuration, effectiveness value was in range of 0.05 to 0.3.

4.2. Energy efficiency and energy density

Table 7 provides a comparison of efficiencies of all encapsulation systems for both experimental configurations. Storage efficiencies have also been mentioned before in above sections while discussing the stored and released energy amount for both layouts. In this section, a summary of results is being provided in terms of storage efficiency and energy density. Storage efficiency is calculated as given below in Eq. (3):

$$Storage\ efficiency = \frac{(Q_{water} + Q_{PCM})_{recovered}}{(Q_{water} + Q_{PCM})_{stored}} \tag{3}$$

For layout 1, FlatICE managed to extract 84 % of the stored energy while both TubeICE and ThinICE configurations managed to recover 80 % of the stored energy. For layout 2, the storage efficiencies are quite close to each other for all encapsulations as TubeICE has storage efficiency of 82 % followed by ThinICE (81 %), and Flat ICE (78 %). For layout 1, the storage efficiency for ThinICE and TubeICE are same thus important factor to choose any encapsulation design becomes the time taken by a certain encapsulation system for charging and discharging. Similarly, in layout 2, there isn't huge difference in storage efficiencies. Thus important factors to choose an encapsulation design will be the

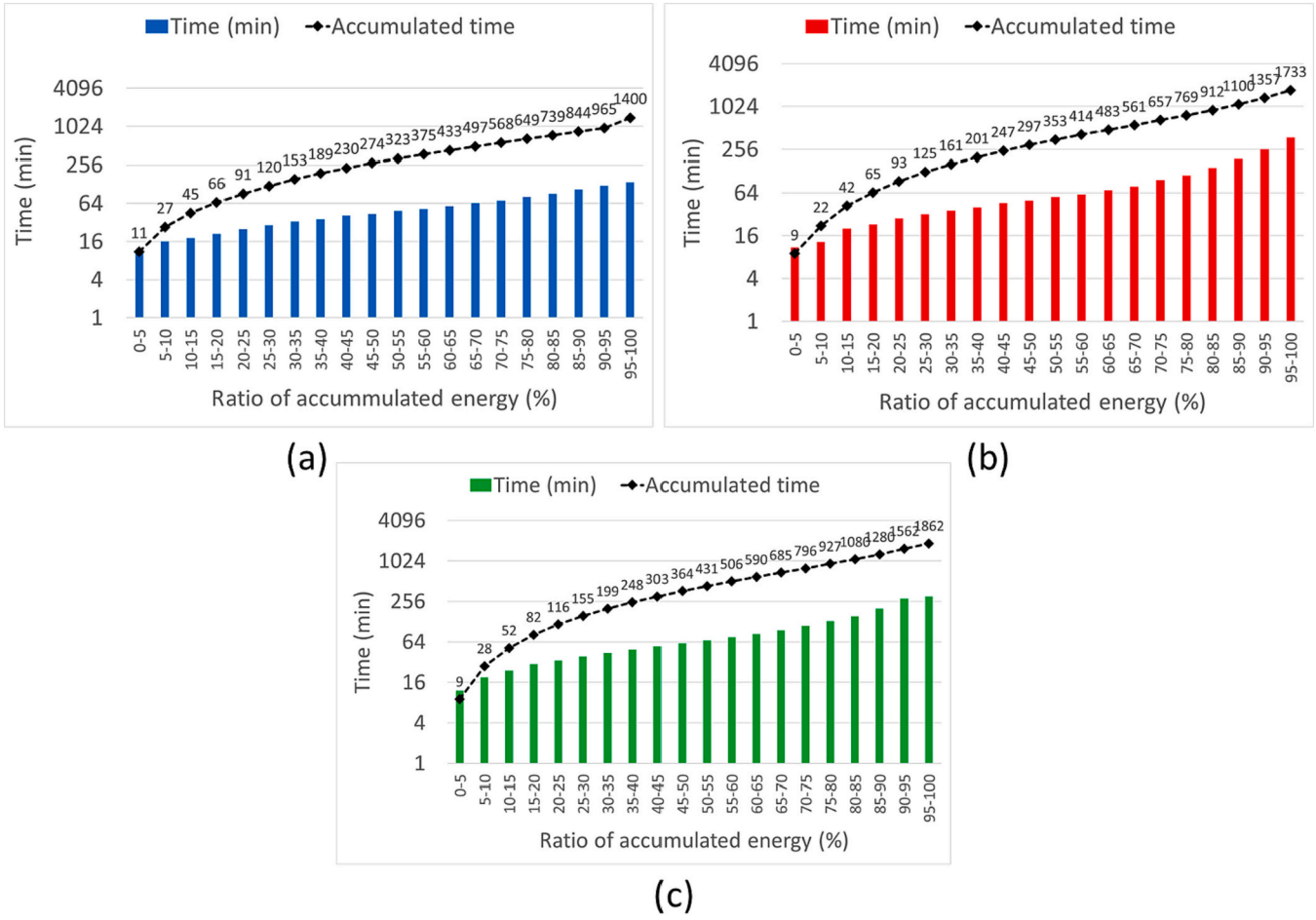

Fig. 19. Ratio of accumulated energy (%) (in bars) in terms of time (accumulated time in dashed line) (a) ThinICE (b) TubeICE (c) FlatICE.

Table 6
Effectiveness of charging process for encapsulations for both experimental layouts.

Encapsulation	Effectiveness (ε)	
	Layout 1	Layout 2
ThinICE	0.82	0.82
TubeICE	0.96	0.78
FlatICE	0.81	0.62

Table 7
Storage efficiency of encapsulations for both experimental layouts.

Encapsulation	Storage efficiency	
	Layout 1	Layout 2
ThinICE	80 %	81 %
TubeICE	80 %	82 %
FlatICE	84 %	78 %

charging and discharging times and amount of energy stored as per application requirement. A study carried out by Suresh and Saini [51] performed an experimental study on combined sensible-latent heat storage system for different volume fractions of PCM spherical molecules. The values of storage efficiencies reported for 80 %, 60 %, 40 % and 20 % volume fractions were 93 %, 90 %, 94 % and 87 % respectively. Gao et al. [52] performed thermal performance analysis of sensible and latent TES tanks and reported 66 % storage efficiency while using latent TES tank.

Table 8 presents storage densities for all encapsulation types for both experimental configurations. Storage density is calculated as given in Eq. (4) where V_{tank} stands for volume of tank. For layout 1, FlatICE reported highest storage density followed by ThinICE and TubeICE respectively. For layout 2 however, TubeICE reported higher storage density than ThinICE mainly because of higher energy recovery. FlatICE reported maximum storage density in both configurations.

$$Storage\ density = \frac{(Q_{water} + Q_{PCM})_{recovered}}{V_{tank}} \quad (4)$$

Table 9 shows the storage density in terms of PCM mass inside the tank. It is calculated as given in Eq. (5) where m_{PCM} stands for mass of PCM inside the tank. For layout 1, ThinICE and FlatICE reported similar values for storage densities. For layout 2, ThinICE reported highest value for storage density followed by FlatICE and TubeICE. TubeICE has highest amount of PCM inside the tank in layout 2 and thus returned lower value for storage density.

$$Storage\ density = \frac{(Q_{water} + Q_{PCM})_{recovered}}{m_{PCM}} \quad (5)$$

Table 8
Storage density (kWh/m^3) of encapsulations for both experimental layouts.

Encapsulation	Storage density (kWh/m^3)	
	Layout 1	Layout 2
ThinICE	27.9	27.9
TubeICE	26.3	32.3
FlatICE	28.6	33.1

Table 9
Storage density (kWh/kg) of encapsulations for both experimental layouts.

Encapsulation	Storage density (kWh/kg)	
	Layout 1	Layout 2
ThinICE	0.09	0.09
TubeICE	0.08	0.05
FlatICE	0.09	0.06

Considering effectiveness, charging efficiency and storage density, the use of FlatICE with layout 1 is recommended.

5. Conclusions

Macro-encapsulation is a highly prevalent and practical technique employed in thermal energy storage (TES) systems due to its feasibility in manufacturing and cost-effectiveness. However, the impact of macro-encapsulation on the performance of latent heat thermal energy storage systems lacks experimental evidence in the existing literature. This paper aims to address this research gap by conducting a comprehensive analysis of the thermal behaviour of three encapsulation designs (rectangular and cylindrical shapes): ThinICE, TubeICE, and FlatICE. The investigation focuses on parameters such as energy storage, energy release, as well as charging and discharging durations to provide valuable insights into the performance of these macro-encapsulation designs for latent heat TES applications.

The results clearly demonstrate that the design of the encapsulation has a direct influence on the thermal behaviour and performance of the energy system. Consequently, when considering specific application requirements, it is crucial to take into account the relevant design parameters. This knowledge will enable informed decision-making and the selection of suitable encapsulation designs to enhance the overall efficiency and effectiveness of energy storage systems.

The phase change material used for this study is PlusICE S17 which is a salt hydrate. A heat loss test is also carried out to cater heat losses in the calculations. Two experimental configurations have been proposed; one with similar storage capacity while other with maximum packing factor configuration. For first layout, specially designed spacers are used to make sure the uniform distribution of PCM inside the tank. For second layout, TubeICE allowed higher mass to be incorporated in the tank followed by FlatICE and TubeICE respectively. TubeICE reported highest effectiveness value for layout 1 while ThinICE reported highest effectiveness value for layout 2.

For layout 1, TubeICE provides higher power for shortage period of time while ThinICE and FlatICE provide stable power for longer period of time. Moreover, FlatICE managed to recover 84 % of the stored energy while rest of the two encapsulations managed to recover 80 % of the stored energy. Furthermore, FlatICE reported highest storage density in terms of volume followed by ThinICE and TubeICE respectively. FlatICE and ThinICE reported similar storage densities in terms of mass.

Compared to sensible storage, given a temperature difference of 20 K, ThinICE and FlatICE configurations demonstrated an approximate 20 % increase in energy discharge, whereas TubeICE showed a relatively smaller increase of around 12 % in energy discharge.

For layout 2, TubeICE and FlatICE provide stable power for longer time period while ThinICE provided higher power for short period of time. Therefore, for the applications requiring stable power for a longer time period, TubeICE and FlatICE in maximum packing factor configuration will be more suitable. TubeICE released 82 % of stored energy followed by ThinICE and FlatICE which released 81 % and 78 % of stored energy respectively. Furthermore, FlatICE reported highest storage density in terms of volume followed by TubeICE and ThinICE respectively. ThinICE reported highest storage density in terms of mass followed by FlatICE and TubeICE, respectively.

When compared to water storage alone, these encapsulation designs demonstrated energy storage improvements of approximately 48 %, 68 %, and 82 % respectively. Moreover, the TES tanks associated with ThinICE, TubeICE, and FlatICE exhibited energy release levels that surpassed those of sensible storage by 19 %, 38 %, and 41 % respectively.

The results are discussed in the context of the epsilon-NTU method. The charging effectiveness of all the configurations is calculated and compared to values reported in the literature. Among the layouts considered, TubeICE demonstrated the highest effectiveness in layout 1, while ThinICE exhibited the highest charging effectiveness in layout 2.

Indeed, the selection of macro-encapsulation designs is highly dependent on the specific application requirements. Additionally, the requirement for stable power over an extended duration or higher power within a shorter period can influence the choice of encapsulation design.

Taking into account effectiveness, charging efficiency, and storage density criteria, it is recommended to utilize FlatICE with layout 1. This design demonstrates favorable characteristics that align with the specified criteria, making it a suitable choice for the given application. However, it is important to conduct a thorough evaluation of the specific requirements and constraints of the application to determine the most optimal encapsulation design.

Nomenclature

thermal energy storage TES
phase change material PCM
phase change materials PCMs
renewable energy resources RES
latent heat thermal energy storage systems LHTES
Reynolds *Re*

CRediT authorship contribution statement

Omais Abdur Rehman: Investigation, Writing – original draft, Visualization. **Valeria Palomba:** Methodology, Validation, Writing – original draft, Supervision. **David Verez:** Conceptualization, Methodology, Investigation, Writing – review & editing. **Emiliano Borri:** Methodology, Formal analysis, Writing – review & editing. **Andrea Frazzica:** Conceptualization, Validation, Formal analysis, Writing – review & editing, Supervision. **Vincenza Brancato:** Methodology, Formal analysis, Writing – review & editing. **Teresa Botargues:** Methodology, Validation, Writing – review & editing. **Zafer Ure:** Conceptualization, Validation, Writing – review & editing. **Luisa F. Cabeza:** Conceptualization, Methodology, Formal analysis, Resources, Data curation, Writing – review & editing, Supervision, Project administration, Funding acquisition.

Declaration of competing interest

The authors declare that they have no known competing financial interests or personal relationships that could have appeared to influence the work reported in this paper.

Data availability

Data will be made available on request.

Acknowledgments

This project was funded by the European Union's Horizon 2020 Research and Innovation Programme under No. 101007976 (CO-COOL). This work is partially supported by ICREA under the ICREA Academia programme. This work is also partially funded by Ministerio de Ciencia e Innovación—Agencia Estatal de Investigación (AEI) (PID2021-123511OB-C31 - MCIN/AEI/10.13039/501100011033/FEDER, EU and RED2022-134219-T). The authors at the University of Lleida would like to thank the Catalan Government for the quality accreditation given to

their research group GREiA (2021 SGR 01615). GREiA is a certified agent TECNIO in the category of technology developers from the Government of Catalonia.

Appendix A

Uncertainty analysis

An uncertainty analysis is carried out for power to calculate the impact of uncertainty associated with the sensors used in these experiments. Uncertainty analysis helps in ensuring the accuracy of results. The analysis was carried out using GUM methodology [53] which is exemplified in [54]. The uncertainty of involved parameters is given in table below. Based on available data Eq. (1) is used and uncertainty for power delivered by tank is obtained as 3.5 %.

Table 10
Uncertainty for HTF parameters.

Parameter	Uncertainty
Density	0.0002 % [55]
Volumetric flow rate	0.25 % [56]
Specific heat capacity	1.5 % [57]

$$u\left(\dot{E}_{HTF}\right) = \left[\left[\frac{\delta\dot{E}}{\delta\rho}u(\rho_{HTF})\right]^2 + \left[\frac{\delta\dot{E}}{\delta\dot{V}}u\left(\dot{V}_{HTF}\right)\right]^2 + \left[\frac{\delta\dot{E}}{\delta C_p}u\left(C_{p\,HTF}\right)\right]^2 + \left[\frac{\delta\dot{E}}{\delta\Delta T_{HTF}}u(\Delta T_{HTF})\right]^2\right]^{0.5} \quad (1)$$

Energy equations

Theoretical energy in Tables 4 and 5 is calculated using following Eqs. (2) and (3). Equations to calculate U value and energy losses are given as Eqs. (4) and (5).

$$Q_{PCM} = \left(m_{PCM}\cdot C_{p\,PCM}\cdot\Delta T\right) + \left(m_{PCM}\cdot h_{PCM}\right) + \left(m_{PCM}\cdot C_{p\,PCM}\cdot\Delta T\right) \quad (2)$$

$$Q_{water} = \left(m_{water}\cdot C_{p\,water}\cdot\Delta T\right) \quad (3)$$

$$U = E_{losses}/\left(A\cdot\Delta t\cdot\Delta T_{LMTD}\right) \quad (4)$$

$$\dot{E}_{losses} = U\cdot A\cdot\Delta T_{LMTD} \quad (5)$$

$$Storage\ efficiency = \frac{\left(\left(m_{water}\cdot C_{p\,water}\cdot\Delta T\right) + \left(m_{PCM}\cdot C_{p\,PCM}\cdot\Delta T\right)_{sensible} + \left(m_{PCM}\cdot h_{PCM}\right)_{latent}\right)_{recovered}}{\left(\left(m_{water}\cdot C_{p\,water}\cdot\Delta T\right) + \left(m_{PCM}\cdot C_{p\,PCM}\cdot\Delta T\right)_{sensible} + \left(m_{PCM}\cdot h_{PCM}\right)_{latent}\right)_{stored}} \quad (6)$$

$$\dot{Q}_{charging} = \left(\dot{m}_{water}\cdot C_{p\,water}\cdot\left(T_{tank\_inlet} - T_{tank\_outlet}\right)\right) \quad (7)$$

$$\dot{Q}_{discharging} = \left(\dot{m}_{water}\cdot C_{p\,water}\cdot\left(T_{tank\_inlet} - T_{tank\_outlet}\right)\right) \quad (8)$$

In Eqs. (2) and (3) above, m is for mass, Cp for specific heat capacity and h is for latent heat capacity of PCM.

In Eqs. (4) and (5), UA is heat loss coefficient, A is surface area of TES tank, Δt is time in seconds and ΔT_{LMTD} is log mean temperature difference.

The equation used to calculate storage efficiency (Eq. (3) in text) is actually a ratio of recovered to stored energy. Both numerator and denominator contain addition of energy stored by water and PCM as given in Eq. (6) above.

Eqs. (7) and (8) are used to calculate charging and discharging powers for both configurations. The details about mass flowrate and other parameters involved are given in Section 2.4.

References

[1] O.A. Rehman, V. Palomba, A. Frazzica, A. Charalampidis, S. Karellas, L.F. Cabeza, Numerical and experimental analysis of a low-GWP heat pump coupled to electrical and thermal energy storage to increase the share of renewables across Europe, Sustain 15 (6) (Mar. 2023) 4973, https://doi.org/10.3390/SU15064973, 2023, Vol. 15, Page 4973.

[2] P. Moreno, A. Castell, C. Solé, G. Zsembinszki, L.F. Cabeza, PCM thermal energy storage tanks in heat pump system for space cooling, Energy Build. 82 (Oct. 2014) 399–405, https://doi.org/10.1016/J.ENBUILD.2014.07.044.

[3] O.A. Rehman, V. Palomba, A. Frazzica, L.F. Cabeza, Enabling technologies for sector coupling: a review on the role of heat pumps and thermal energy storage, Energies 14 (24) (Dec. 2021) 8195, https://doi.org/10.3390/EN14248195, 2021, Vol. 14, Page 8195.

[4] C. Prieto, S. Fereres, L. Cabeza, The role of innovation in industry product deployment: Developing thermal energy storage for concentrated solar power, Energies 13 (11) (Jun. 2020), https://doi.org/10.3390/en13112943.

[5] K. Rajendran, J. Ling-Chin, A.P. Roskilly, Thermal energy efficiency in industrial processes, in: Handb. Clean Energy Syst, Jul. 2015, pp. 1–30, https://doi.org/10.1002/9781118991978.HCES091.

[6] H. Selvnes, Y. Allouche, R.I. Manescu, A. Hafner, Review on cold thermal energy storage applied to refrigeration systems using phase change materials, Therm. Sci. Eng. Prog. 22 (May 2021) 100807, https://doi.org/10.1016/J.TSEP.2020.100807.

[7] Maurice Marongiu, Thermal Management of Electronic Equipment using Phase Change Materials (PCMs) | Electronics Cooling. https://www.electronics-cooling.

com/2019/03/thermal-management-of-electronic-equipment-using-phase-change-materials-pcms/, Mar. 06, 2019. (Accessed 9 June 2023).
[8] K. Huang, et al., Macro-encapsulated PCM cylinder module based on paraffin and float stones, Mater 9 (5) (May 2016) 361, https://doi.org/10.3390/MA9050361, 2016, *Vol. 9, Page 361*.
[9] T.E. Alam, J.S. Dhau, D.Y. Goswami, E. Stefanakos, Macroencapsulation and characterization of phase change materials for latent heat thermal energy storage systems, Appl. Energy 154 (Sep. 2015) 92–101, https://doi.org/10.1016/J.APENERGY.2015.04.086.
[10] Z. Liu, et al., A review on macro-encapsulated phase change material for building envelope applications, Build. Environ. 144 (Oct. 2018) 281–294, https://doi.org/10.1016/J.BUILDENV.2018.08.030.
[11] A.M. Khudhair, M.M. Farid, A review on energy conservation in building applications with thermal storage by latent heat using phase change materials, Energy Convers. Manag. 45 (2) (Jan. 2004) 263–275, https://doi.org/10.1016/S0196-8904(03)00131-6.
[12] L. Yang, et al., A comprehensive review on sub-zero temperature cold thermal energy storage materials, technologies, and applications: state of the art and recent developments, Appl. Energy 288 (Apr. 2021), https://doi.org/10.1016/J.APENERGY.2021.116555.
[13] A.F. Regin, S.C. Solanki, J.S. Saini, Heat transfer characteristics of thermal energy storage system using PCM capsules: a review, Renew. Sust. Energ. Rev. 12 (9) (Dec. 2008) 2438–2458, https://doi.org/10.1016/J.RSER.2007.06.009.
[14] L. Erlbeck, et al., Adjustment of thermal behavior by changing the shape of PCM inclusions in concrete blocks, Energy Convers. Manag. 158 (Feb. 2018) 256–265, https://doi.org/10.1016/J.ENCONMAN.2017.12.073.
[15] L. Navarro, C. Barreneche, A. Castell, D.A.G. Redpath, P.W. Griffiths, L.F. Cabeza, High density polyethylene spheres with PCM for domestic hot water applications: water tank and laboratory scale study, J. Energy Storage 13 (Oct. 2017) 262–267, https://doi.org/10.1016/J.EST.2017.07.025.
[16] A. Barba, M. Spiga, Discharge mode for encapsulated PCMs in storage tanks, Sol. Energy 74 (2) (Feb. 2003) 141–148, https://doi.org/10.1016/S0038-092X(03)00117-8.
[17] Q. Al-Yasiri, M. Szabó, Thermal performance of concrete bricks based phase change material encapsulated by various aluminium containers: an experimental study under Iraqi hot climate conditions, J. Energy Storage 40 (Aug. 2021) 102710, https://doi.org/10.1016/J.EST.2021.102710.
[18] K.A.R. Ismail, R.I.R. Moraes, A numerical and experimental investigation of different containers and PCM options for cold storage modular units for domestic applications, Int. J. Heat Mass Transf. 52 (19–20) (Sep. 2009) 4195–4202, https://doi.org/10.1016/J.IJHEATMASSTRANSFER.2009.04.031.
[19] A. Heinz, C. Moser, Numerical modelling and experimental testing of a thermal storage system with non-spherical macro-encapsulated phase change material modules, J. Energy Storage 58 (Feb. 2023) 106427, https://doi.org/10.1016/J.EST.2022.106427.
[20] D. Vérez, et al., Experimental study on two PCM macro-encapsulation designs in a thermal energy storage tank, Appl. Sci. 11 (13) (Jul. 2021) 6171, https://doi.org/10.3390/APP11136171. *2021, Vol. 11, Page 6171*.
[21] K. Faraj, M. Khaled, J. Faraj, F. Hachem, C. Castelain, Phase change material thermal energy storage systems for cooling applications in buildings: a review, Renew. Sust. Energ. Rev. 119 (Mar. 2020) 109579, https://doi.org/10.1016/J.RSER.2019.109579.
[22] J. Dallaire, H.M. Adeel Hassan, J.H. Bjernemose, M.P. Rudolph Hansen, I. Lund, C. T. Veje, Performance analysis of a dual-stack air-PCM heat exchanger with novel air flow configuration for cooling applications in buildings, Build. Environ. 223 (Sep. 2022) 109450, https://doi.org/10.1016/J.BUILDENV.2022.109450.
[23] S. Zhang, S. Mancin, L. Pu, A review and prospective of fin design to improve heat transfer performance of latent thermal energy storage, J. Energy Storage 62 (Jun. 2023) 106825, https://doi.org/10.1016/J.EST.2023.106825.
[24] R. De Césaro Oliveski, F. Becker, L.A.O. Rocha, C. Biserni, G.E.S. Eberhardt, Design of fin structures for phase change material (PCM) melting process in rectangular cavities, J. Energy Storage 35 (Mar. 2021) 102337, https://doi.org/10.1016/J.EST.2021.102337.
[25] X. Dong, et al., Investigation on heat transfer and phase transition in phase change material (PCM) balls and cold energy storage tank, J. Energy Storage 50 (Jun. 2022) 104695, https://doi.org/10.1016/J.EST.2022.104695.
[26] A. Sharma, H.B. Kothadia, S. Singh, B. Mondal, Solidification of nanoparticle-based PCM in a fin-aided triplex-tube energy storage system for cooling applications, Therm. Sci. Eng. Prog. 42 (Jul. 2023) 101872, https://doi.org/10.1016/J.TSEP.2023.101872.
[27] Y. Ding, H. Wang, B. Huang, Y. Hu, F. Jiang, X. Ling, Thermal performance analysis of a 20-feet latent cold energy storage device integrated with a novel fin-plate unit for building cooling, Renew. Energy 200 (Nov. 2022) 405–418, https://doi.org/10.1016/J.RENENE.2022.09.130.
[28] G. Bejarano, J.J. Suffo, M. Vargas, M.G. Ortega, Novel scheme for a PCM-based cold energy storage system. Design, modelling, and simulation, Appl. Therm. Eng. 132 (Mar. 2018) 256–274, https://doi.org/10.1016/J.APPLTHERMALENG.2017.12.088.
[29] A. Anand, A.S. Purandare, S. Vanapalli, Performance improvement of a PCM cold box by two bilayers configuration, Int. Commun. Heat Mass Transf. 134 (May 2022) 105978, https://doi.org/10.1016/J.ICHEATMASSTRANSFER.2022.105978.
[30] K. Mehalaine, D. Lafri, Improving the energy release of a latent heat storage with multiple phase change materials loading and partition shaping, Appl. Therm. Eng. 230 (Jul. 2023) 120679, https://doi.org/10.1016/J.APPLTHERMALENG.2023.120679.
[31] N. Bianco, A. Fragnito, M. Iasiello, G.M. Mauro, L. Mongibello, Multi-objective optimization of a phase change material-based shell-and-tube heat exchanger for cold thermal energy storage: experiments and numerical modeling, Appl. Therm. Eng. 215 (Oct. 2022) 119047, https://doi.org/10.1016/J.APPLTHERMALENG.2022.119047.
[32] A. Soh, Z. Huang, W. Chen, M.R. Islam, K.J. Chua, Design optimization of low-temperature latent thermal energy storage for urban cooling applications, Appl. Therm. Eng. 230 (Jul. 2023) 120711, https://doi.org/10.1016/J.APPLTHERMALENG.2023.120711.
[33] 7 Wine-Storage Basics You Need to Know | Wine Spectator. https://www.winespectator.com/articles/how-to-store-wine-temperature-humidity-coolers-and-more. (Accessed 8 June 2023).
[34] Precaution, proof and pragmatism: evolving perspectives on the museum environment (article). https://www.getty.edu/conservation/publications_resources/newsletters/29_2/evolving_perspectives.html. (Accessed 8 June 2023).
[35] ASHRAE, 2021 Equipment Thermal Guidelines for Data Processing Environments, Norcross. [Online]. Available: https://www.ashrae.org/file library/technical resources/bookstore/supplemental files/referencecard_2021thermalguidelines.pdf, 2021. (Accessed 8 June 2023).
[36] Food preservation temperatures and shelf life | HAM Systems | Blog. https://blog.hamsystems.eu/food-preservation-temperatures-and-shelf-life/. (Accessed 8 June 2023).
[37] What Is the Optimal Temperature for a Greenhouse?. https://www.familyhandyman.com/article/what-is-the-optimal-temperature-for-a-greenhouse/. (Accessed 8 June 2023).
[38] Y. Jiang, X. Liu, L. Zhang, T. Zhang, High temperature cooling and low temperature heating in buildings of EBC annex 59, Energy Procedia 78 (Nov. 2015) 2433–2438, https://doi.org/10.1016/J.EGYPRO.2015.11.222.
[39] PCM Products. https://www.pcmproducts.net/. (Accessed 18 April 2023).
[40] PLUSICE Range. https://www.pcmproducts.net/files/PlusICE Range 2021-1.pdf. (Accessed 4 May 2023).
[41] División de refrigeración fija - Zanotti Appliance. https://zanottiappliance.com/es/refrigeracion/refrigeracion-fija/. (Accessed 5 December 2022).
[42] Immersion resistors. http://www.resistenciasasturgo.com/wp-content/uploads/2011/11/Ficha-producto_08.pdf. (Accessed 18 April 2023).
[43] InduSoft Web Studio is now AVEVA Edge – a new name and an exciting opportunity. https://www.aveva.com/en/perspectives/blog/indusoft-web-studio-is-now-aveva-edge/. (Accessed 18 April 2023).
[44] STEP Store. https://store.stepsl.com/product?prod=DL-01. (Accessed 5 December 2022).
[45] C.A. Cruickshank, S.J. Harrison, Heat loss characteristics for a typical solar domestic hot water storage, Energy Build. 42 (10) (Oct. 2010) 1703–1710, https://doi.org/10.1016/J.ENBUILD.2010.04.013.
[46] D. Vérez, et al., Experimental Study of a Small-size Vacuum Insulated Water Tank for Building Applications, 2021, https://doi.org/10.3390/su13105329.
[47] J. Gasia, A. de Gracia, G. Peiró, S. Arena, G. Cau, L.F. Cabeza, Use of partial load operating conditions for latent thermal energy storage management, Appl. Energy 216 (Apr. 2018) 234–242, https://doi.org/10.1016/J.APENERGY.2018.02.061.
[48] A. Sari, K. Kaygusuz, "Thermal performance of palmitic acid as a phase change energy storage material,", Accessed: May 23, 2023. [Online] 43 (6) (2002) 863–876, https://doi.org/10.1016/S0196-8904(01)00071-1. Available: www.elsevier.com/locate/enconman.
[49] N.H.S. Tay, M. Belusko, F. Bruno, An effectiveness-NTU technique for characterising tube-in-tank phase change thermal energy storage systems, Appl. Energy 91 (1) (Mar. 2012) 309–319, https://doi.org/10.1016/J.APENERGY.2011.09.039.
[50] N.A. Aziz, N.A.M. Amin, M.S.A. Majid, F. Bruno, M. Belusko, Optimising a packed bed phase change material of spheres using effectiveness-number of transfer unit method, J. Energy Storage 49 (May 2022) 104019, https://doi.org/10.1016/J.EST.2022.104019.
[51] C. Suresh, R.P. Saini, Experimental study on combined sensible-latent heat storage system for different volume fractions of PCM, Sol. Energy 212 (Dec. 2020) 282–296, https://doi.org/10.1016/J.SOLENER.2020.11.013.
[52] Y. Gao, et al., Thermal performance analysis of sensible and latent heat thermal energy storage tanks: a contrastive experiment, J. Build. Eng. 32 (Nov. 2020) 101713, https://doi.org/10.1016/J.JOBE.2020.101713.
[53] JCGM, GUM-6:2020 Guide to the expression of uncertainty in measurement-Part 6: Developing and using measurement models Guide pour l'expression de l'incertitude de mesure-Partie 6: Élaboration et utilisation des modèles de mesure, JCGM, 2020.
[54] B.D. Mselle, G. Zsembinszki, D. Vérez, E. Borri, L.F. Cabeza, A detailed energy analysis of a novel evaporator with latent thermal energy storage ability, Appl. Therm. Eng. 201 (Jan. 2022) 117844, https://doi.org/10.1016/J.APPLTHERMALENG.2021.117844.
[55] H. Wolf, Determination of water density: limitations at the uncertainty level of 1 × 10-6, Accred. Qual. Assur. 13 (10) (Oct. 2008) 587–591, https://doi.org/10.1007/S00769-008-0442-2/METRICS.
[56] ModMag | Medidor de flujo electromagnético M1000 | Badger Meter. https://www.badgermeter.com/es-es/productos/medidores/medidores-de-flujo-electromagneticos/medidor-de-flujo-electromagnetico-modmag-m1000/. (Accessed 18 April 2023).
[57] S. Rudtsch, Uncertainty of heat capacity measurements with differential scanning calorimeters, Thermochim. Acta 382 (1–2) (Jan. 2002) 17–25, https://doi.org/10.1016/S0040-6031(01)00730-4.